Anisotropic thermal expansion and magnetostriction of YNi_2B_2C single crystals

2006 J. Phys.: Condens. Matter 18 8353

(http://iopscience.iop.org/0953-8984/18/35/020)

INSTITUTE OF PHYSICS PUBLISHING JOURNAL OF PHYSICS: CONDENSED MATTER

J. Phys.: Condens. Matter **18** (2006) 8353–8365 doi:10.1088/0953-8984/18/35/020

Anisotropic thermal expansion and magnetostriction of YNi_2B_2C single crystals

S L Bud'ko[1], G M Schmiedeshoff[2], G Lapertot[1,3] and P C Canfield[1]

[1] Ames Laboratory US DOE and Department of Physics and Astronomy, Iowa State University, Ames, IA 50011, USA
[2] Department of Physics, Occidental College, Los Angeles, CA 90041, USA
[3] Commissariat á l'Energie Atomique, DRFMC-SPSMS-IMAPEC, 38054 Grenoble, France

Received 28 June 2006
Published 18 August 2006
Online at stacks.iop.org/JPhysCM/18/8353

Abstract

We present results of anisotropic thermal expansion and low temperature magnetostriction measurements on YNi_2B_2C single crystals grown by high temperature flux and floating zone techniques. Quantum oscillations of magnetostriction were observed at low temperatures for $H \parallel c$ starting at fields significantly below H_{c2} ($H < 0.7H_{c2}$). Large irreversible, longitudinal magnetostriction was seen in both in-plane and along the c axis directions of the applied magnetic field in the mixed superconducting state. Anisotropic uniaxial pressure dependences of T_c were evaluated using results of zero field, thermal expansion measurements.

1. Introduction

The members of the RNi_2B_2C (R = Gd–Lu, Y) series of compounds serve as model systems for studies of a number of phenomena: coexistence of local moment magnetism and superconductivity, non-locality and flux line lattice transitions, heavy fermion physics and complex metamagnetism [1–4]. Although many sophisticated experiments were performed on RNi_2B_2C borocarbides, data on thermal expansion (TE) and magnetostriction (MS) for several members of the series exist only for limited temperature ranges, or only on polycrystalline samples, or are not available at all. For one of the less complex members of the series, non-magnetic, superconducting YNi_2B_2C, for example, only a rather limited set of results has been disseminated [5–7]. In this publication we report anisotropic (c axis and ab plane) TE and longitudinal, low temperature, MS measurements on YNi_2B_2C single crystals grown by two different techniques and well characterized by other methods. The objective for this work is manifold: to acquire data that can serve as a baseline in studies of TE in more complex, magnetic or strongly correlated, borocarbides; to probe the irreversible properties in mixed superconducting state; and finally, to evaluate the uniaxial pressure derivatives of YNi_2B_2C from the anomalies in TE at T_c (using the thermodynamic Ehrenfest relation), an approach

proven viable e.g. in HTSC [8, 9], and compare the results with the implications of the analysis in [10].

2. Experimental methods

Two YNi_2B_2C single crystals were used in this work. One of them (sample A throughout the rest of the text) was grown by a Ni_2B high temperature flux method (see [1, 11, 12] for more details). This method yields plate-like crystals with the c axis perpendicular to the plates. The crystal was shaped into a nearly rectangular bar, with two pairs of parallel surfaces, so that TE and MS were measured along [100] ($L = 2.37$ mm) and [001] ($L = 0.92$ mm) directions. Another crystal (sample B) was grown using vertical zone melting method with a commercial four-mirror image furnace (model FZ-T-4000-H-VI-VPM-PC, Crystal Systems Corp., Japan). We used drop cast polycrystalline rods (∼6 mm diameter, ∼60 mm long) as feeding rod and crystal support. High purity argon at atmospheric pressure was used as a protective atmosphere inside the quartz working tube. Feeding and bottom shafts were rotated in opposite directions to insure an effective stirring of the molten zone, typically at +10 and −35 rpm. During the growth, the growth speed was decreased from 10 to 2 mm h^{-1} to favour the formation of large, single grains. The phase purity of the single crystals was checked by Debye–Sherrer powder diffraction pattern and compared to original feeding rod spectrum. No detectable extra reflections due to impurity phases or changes of cell parameters were observed. An as-grown bar was oriented with a Laue camera and cut into a close to prismoidal shape with two pairs of parallel surfaces, so that TE and MS were measured along [110] ($L = 3.03$ mm) and [001] ($L = 1.82$ mm) directions. After shaping, both samples were annealed in dynamic vacuum (10^{-5}–10^{-6} Torr) at 950 °C [13]. It should be mentioned that for reasons unrelated to the objectives of this work, the sample A was grown with isotopically pure ^{10}B and the sample B with ^{11}B.

Magnetization measurements were performed using a commercial MPMS-5 (Quantum Design, Inc.) SQUID magnetometer; ac resistance ($f = 16$ Hz, $I = 3$ mA) and heat capacity were measured with ACT and heat capacity options of a PPMS-9 instrument (Quantum Design, Inc.).

Thermal expansion and magnetostriction were measured using a capacitive dilatometer constructed of OFHC copper; a detailed description of the dilatometer will appear elsewhere [14]. The capacitance was measured with an Andeen–Hagerling 2500A capacitance bridge (the bridge resolution of 10^{-7} pF corresponds to a sample dilation measurement limit of about 0.3 pm when the dilatometer is operating near 20 pF). The dilatometer was mounted in a PPMS-14 instrument (Quantum Design Inc.) and was operated over a temperature range of 1.8–305 K and in magnetic fields up to 140 kOe (either in vacuum or with a small amount of helium exchange gas to minimize thermal gradients). The temperature was measured with a calibrated Cernox-1030 thermometer (Lakeshore Cryotronics) mounted on the dilatometer. The field dependence of the dilatometer was less than ±3 Å over ±140 kOe and will be ignored. The temperature dependence of the dilatometer (or 'cell effect') is removed using published values of the thermal expansion of copper [15]. Data were acquired with the temperature increasing at a rate of about 0.4 K min^{-1} or with the field changing at a rate of about 6 kOe min^{-1}. The absolute accuracy of the dilatometer was checked with measurements on a 4 mm sample of pure aluminium that were compared to published values [15]. The average deviation between our aluminium TE measurements and those in the literature over our full temperature range is 7.0×10^{-8} K^{-1}. The average fractional deviation of our aluminium measurements from those in the literature is about 1% above 40 K but becomes larger at low temperatures where the thermal expansion of aluminium is sensitive to both sample purity and preparation [15].

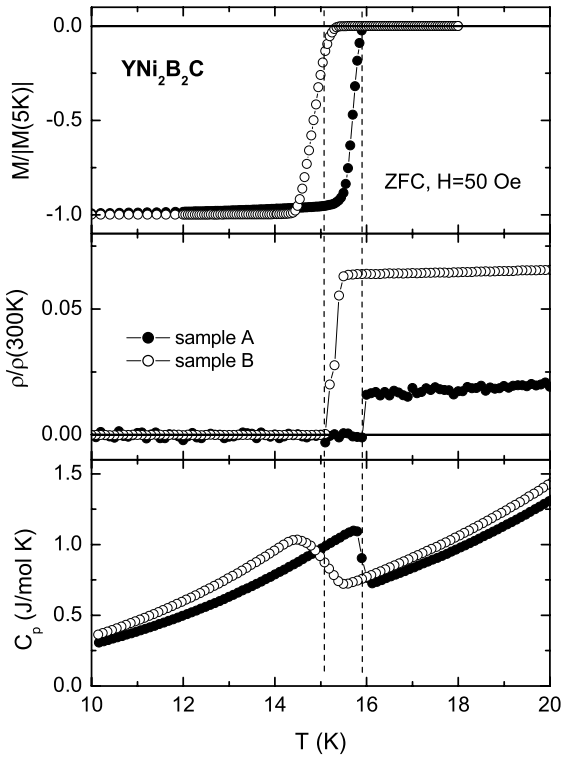

Figure 1. Temperature-dependent magnetization, resistivity and heat capacity for samples A and B near superconducting transition. Vertical lines mark transition as defined by $\rho = 0$.

The maximum deviation of 2.8×10^{-7} K^{-1} occurred at 300 K and corresponds to a fractional deviation of 1.2% from published values. We estimate an experimental uncertainty of 10^{-8} K^{-1} in our thermal expansion measurements from the mean deviation to a fit of our aluminium data near 20 K, this corresponds to a dilation uncertainty less than 0.5 Å K^{-1}.

3. Results and discussion

3.1. Thermal expansion

Superconducting transitions, as measured by DC magnetization, zero field resistivity and heat capacity, are shown in figure 1. In all three measurements the transitions are sharp, being sharper for sample A. The T_c values as defined by $\rho = 0$, onset of diamagnetism in $M(T)$ measurements and mid-point of the heat capacity rise (or by balancing of the normal state and superconducting state entropies) are ∼15.9 K and ∼15.1 K for samples A and B respectively. This difference in T_c between samples A and B is partially due to the boron isotope effect [16, 17] and partially due to different scattering in two samples as can be see from the difference in the residual resistivity ratio, RRR $= \rho(300\text{ K})/\rho(17\text{ K}) \approx 63$ and 16 for A and B respectively [13]. It should be noted that sample B had a small, rather broad, bump in resistivity near 30 K, feature that was not observed in the sample A or other flux grown YNi_2B_2C samples.

Temperature-dependent linear and volume (defined here as $\Delta V/V_0 = \Delta L_c/L_{c0} + 2\Delta L_{ab}/L_{ab0}$) dilations (relative to the values at 1.9 K) for two samples are shown in figure 2.

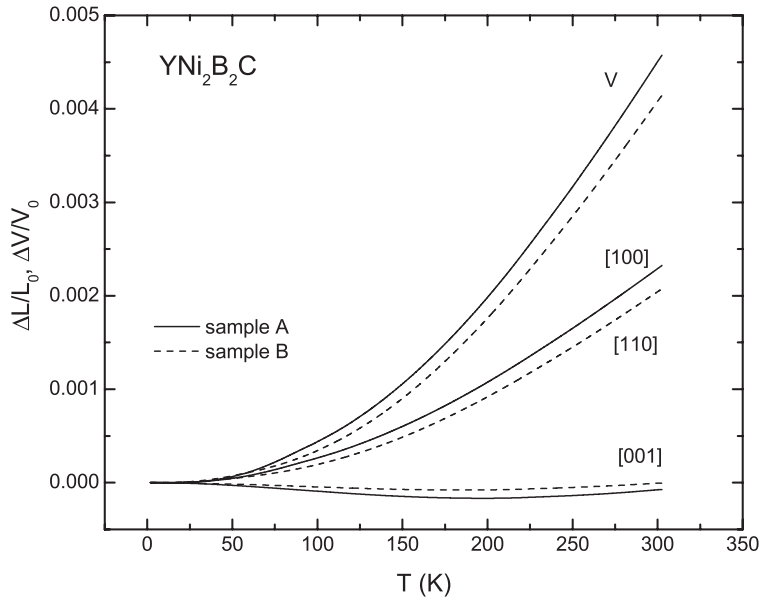

Figure 2. Relative temperature-dependent linear and volume dilations of two YNi_2B_2C crystals.

The two crystals behave very similarly with the slight discrepancy most probably reflecting the accuracy of the measurements of the room temperature dimensions and their changes and possible, slight imperfections in the shape of the samples. In-plane linear and volume thermal dilations are positive in the temperature range studied. The c axis thermal dilation is negative at low temperatures, it changes its sign at about 200 K.

Temperature-dependent linear and volume thermal expansion coefficients measured on samples A and B are shown in figure 3. $\alpha_c(T)$ data for both samples are very similar, as well as the $\alpha_{ab}(T)$ data above ∼100 K. Further studies will be required to understand whether the broad maximum in $\alpha_{[100]}(T)$ of the sample A at about 80 K is a real feature albeit it was reproducible in two consecutive measurements: one in high vacuum mode of the PPMS, another with low pressure He exchange gas in the sample chamber. Our data are compared with the published data [6, 7] obtained by powder and single crystal x-ray diffraction at different temperatures. To be consistent with the figure 3 and results for β in the table 3 of [7], the α_c data cited in [7] for YNi_2B_2C should be divided by 10. Such 'corrected' α_c data together with the α_a and β data from the table 3, reference [7] are included in figure 3. Our data are consistent with the published values [6, 7].

The temperature dependence of the linear thermal expansion coefficients close to T_c is presented in figure 4. Jumps in $\alpha_i(T)$ are seen unambiguously, with the opposite sign of the jumps for α_{ab} and α_c and very similar, within the errors of the measurements, values for both samples. Using results from the heat capacity (figure 1) and thermal expansion coefficients (figure 4) measurements, the uniaxial pressure derivatives of the superconducting transition temperature, T_c, can be calculated using the thermodynamic Ehrenfest relation:

$$\frac{dT_c}{dp_i} = V_{mol} \cdot \Delta\alpha_i(T_c) \cdot \left[\frac{\Delta C_p(T_c)}{T_c}\right]^{-1}$$

where V_{mol} is a molar volume of the material (for YNi_2B_2C, $V_{mol} = 39.5$ cm^3) and $\Delta\alpha_i(T_c)$ and $\Delta C_p(T_c)$ are the jumps in the ith thermal expansion coefficient and specific heat at T_c.

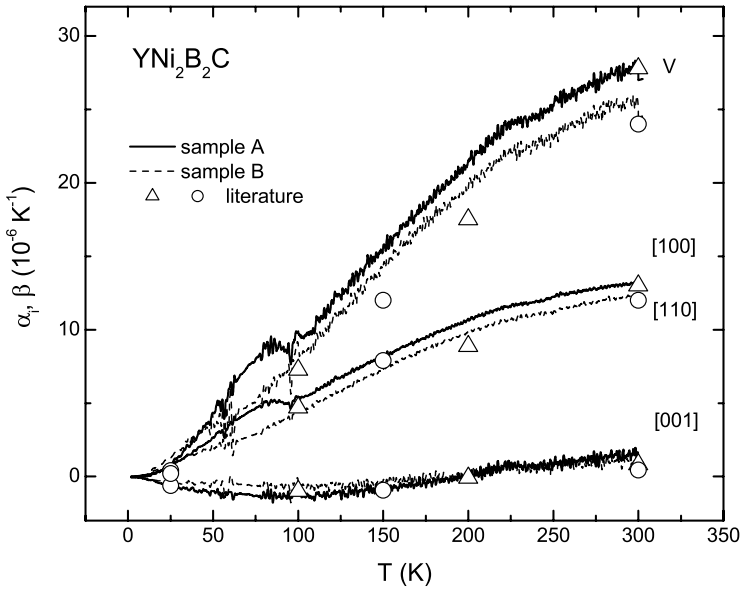

Figure 3. Temperature-dependent linear and volume thermal expansion coefficients for two YNi_2B_2C crystals plotted together with literature data; symbols: ○—[6], △—[7] (see text for discussion of the literature values).

Table 1. Changes in specific heat and thermal expansion coefficients at T_c and estimates of anisotropic pressure derivatives of T_c for two samples of YNi_2B_2C. Sample A: $YNi_2\ ^{10}B_2C$, solution grown, RRR ≈ 63; sample B: $YNi_2\ ^{11}B_2C$, melted zone grown, RRR ≈ 16.

Sample	T_c (K)	ΔC_p (mJ mol^{-1} K^{-1})	$\Delta\alpha_{ab}$ (10^{-8} K^{-1})	$\Delta\alpha_c$ (10^{-8} K^{-1})	dT_c/dp_{ab} (K kbar^{-1})	dT_c/dp_c (K kbar^{-1})	dT_c/dP^* (K kbar^{-1})
A	15.9	444	−7.2	5.9	-1.02×10^{-2}	0.83×10^{-2}	-1.21×10^{-2}
B	15.1	522	−6.5	6.5	-0.74×10^{-2}	0.74×10^{-2}	-0.74×10^{-2}

Estimates of the uniaxial pressure derivatives for YNi_2B_2C based on the aforementioned measurements are summarized in table 1. Within the 10–20% error bars in $\Delta\alpha_i$ (see figure 4) there is no significant difference in estimated uniaxial pressure derivatives for two samples. In the table $dT_c/dP^* = 2 \cdot dT_c/dp_{ab} + dT_c/dp_c$. The dT_c/dP^* defined in such way lacks the contribution from the off-diagonal dT_c/dp_{ij} terms that play a role in the experimentally measured dT_c/dP under hydrostatic pressure. Since the off-diagonal terms are usually significantly smaller then the diagonal ones, we can still compare the last column of the table 1 with the experimentally measured hydrostatic pressure derivatives. The experimental data on dT_c/dP of YNi_2B_2C were presented in a number of publications, some of the reported values are listed below (in K kbar^{-1}): -0.58×10^{-2} [18], -0.9×10^{-2} [19], 0.32×10^{-2} (in $P \to 0$ limit) [20], and -0.9×10^{-2} [21]. All but one of these results are consistent with our estimates. We are unaware of any direct uniaxial pressure measurements on YNi_2B_2C other than very short conference proceedings publication [22], that contains a statement that for this material T_c is almost independent on (uniaxial) pressure, again in agreement with our estimates of dT_c/dp_i (table 1).

The uniaxial pressure derivatives obtained from the Ehrenfest relations in this work differ in value and, more importantly, have the signs opposite to the ones inferred in [10]. The

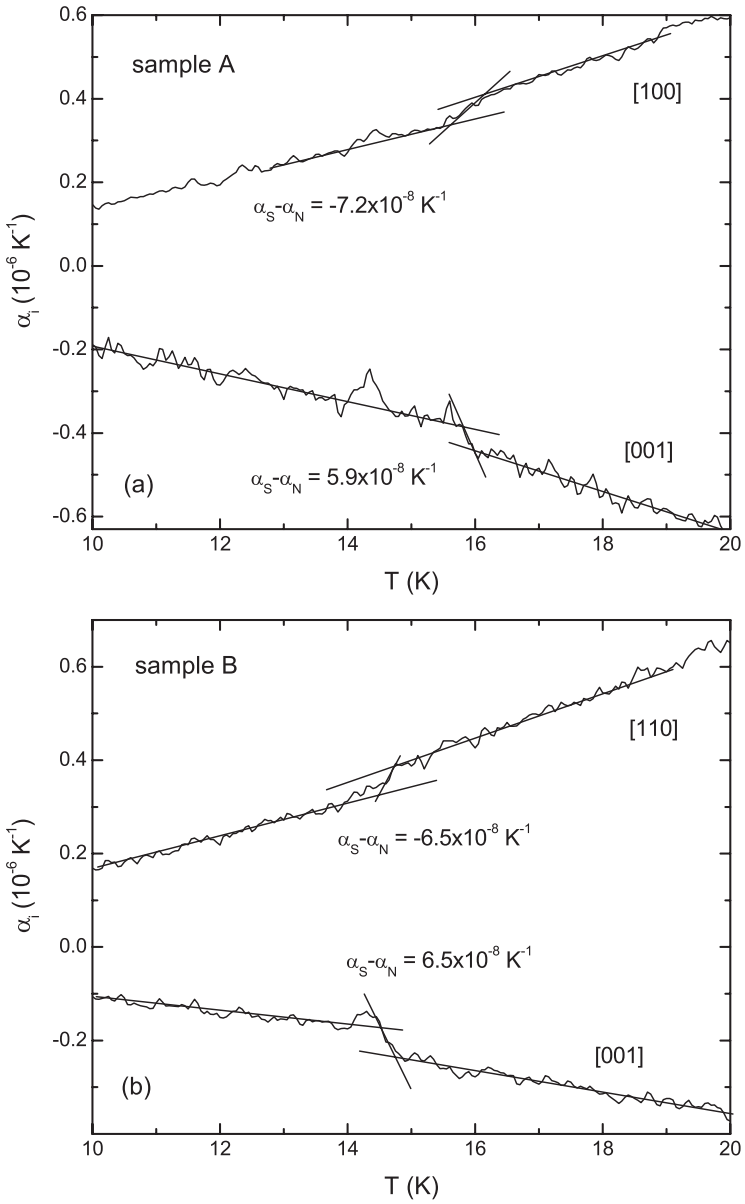

Figure 4. Temperature-dependent linear thermal expansion coefficients for two YNi_2B_2C crystals in the vicinity of the superconducting transition.

procedure used there was indirect, based on a number of assumptions (the most important, but not universally correct, being equivalence of physical and chemical pressure), had to rely (due to the nature of the doping used) on refining of the structural data of two-phase samples, and therefore is open for discussions and criticism. On the other hand, it is noteworthy that additionally our current results (table 1) apparently contradict the implications of the band-structure calculations [23] that superconductivity in RNi_2B_2C is controlled by the static tetrahedral NiB_4 geometry. Within the model of [23] superconductivity is more favourable

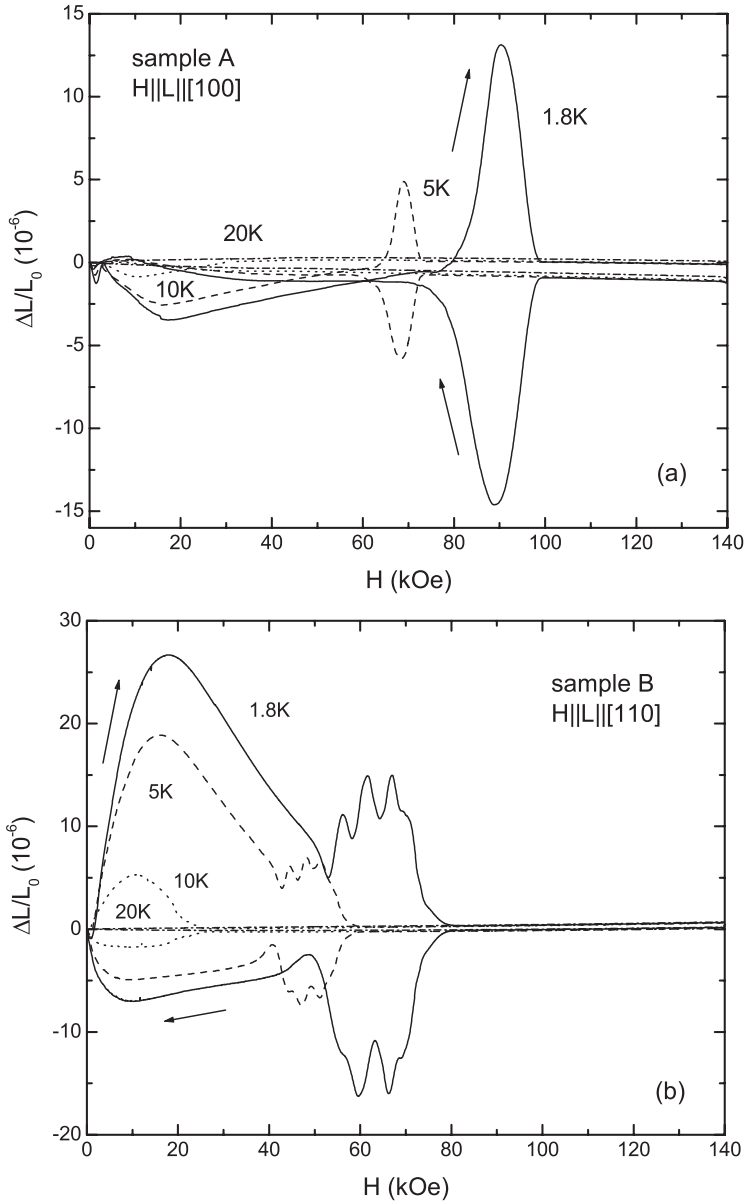

Figure 5. Longitudinal magnetostriction for two YNi_2B_2C crystals with magnetic fields applied in the ab plane. ΔL is defined as $L(H) - L(H = 0)$.

for RNi_2B_2C compounds with the B–Ni–B tetrahedral angle ϕ closer to the ideal value of $\phi_{\text{ideal}} = 109.5°$. For all RNi_2B_2C compounds $\phi < \phi_{\text{ideal}}$ (for YNi_2B_2C $\phi \approx 107.3°$ [6]). Then a compression along the c axis will cause a decrease in ϕ bringing it further away from the ϕ_{ideal}, and in-ab-plane compression will yield an increase in ϕ so that it will approach ϕ_{ideal}, consequently the signs of the uniaxial pressure derivatives of T_c expected from [23] are $dT_c/dp_c < 0$, $dT_c/dp_{ab} > 0$, opposite to that evaluated from the TE experiment (table 1).

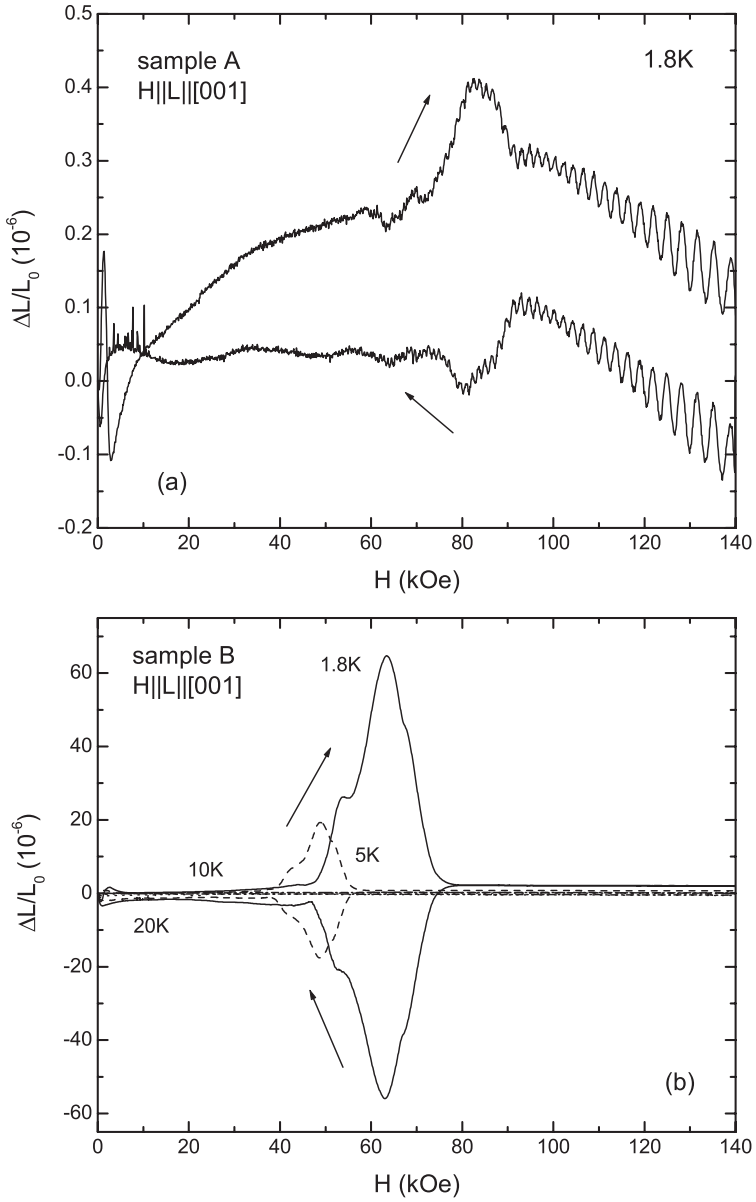

Figure 6. Longitudinal magnetostriction for two YNi_2B_2C crystals with magnetic fields applied along the c axis. For sample A only data at $T = 1.8$ K are shown. ΔL is defined as $L(H) - L(H = 0)$.

3.2. Magnetostriction

Magnetostriction loops taken at different temperatures, both in superconducting and normal state, for field applied in the *ab* plane, are shown in figure 5. Magnetostriction in superconducting state depends on number of parameters, including the extrinsic ones, like shape of the sample, pinning strength and its field dependence [24–27]. Moreover, irreversible flux pinning induced magnetostriction causes (geometry-dependent) shape distortions [26, 28]

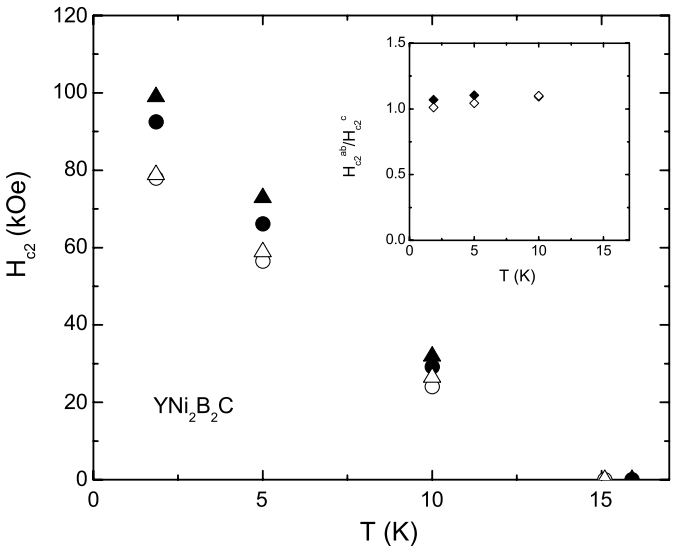

Figure 7. Temperature-dependent H_{c2} for two YNi_2B_2C crystals as defined from magnetostriction measurements. Triangles—$H \parallel ab$, circles—$H \parallel c$, filled symbols—sample A, open symbols—sample B. Inset shows anisotropy of H_{c2}.

that add additional requirements on mounting of the sample in the experimental cell for detailed study of the critical superconducting state via magnetostriction. Here we will just mention that in both samples the magnetostriction in the mixed superconducting state is high ($\Delta L_{max}/L_0 > 1 \times 10^{-7}$), significantly higher than that seen for the polycrystalline sample [5], in both samples the features associated with peak effect [27] or 'dip' in magnetization [29] are apparently seen, with some structure for the sample B. In the normal state magnetostriction is rather small. In superconducting state, for magnetic fields appreciably lower than H_{c2}, the irreversible magnetostriction is much higher for the sample B, consistent with its lower RRR (figure 1) and higher pinning in this sample.

For field applied along c direction the quantitative difference in the irreversible magnetostriction in superconducting state between two samples is even more drastic that for $H \parallel ab$ (figure 6). Very large, ($\Delta L_{max}/L_0 \approx 6 \times 10^{-7}$) effect is seen for sample B and is possibly associated with the peak (and/or 'dip') effect. Much smaller feature in the irreversible magnetostriction is seen below H_{c2} in the sample A.

The magnetostriction data allow for an estimate of the H_{c2} (defined here as the high field onset of the peak/dip effect feature). The anisotropic data for both samples are shown in figure 7. The values of H_{c2} and its anisotropy ($H_{c2}^{ab}/H_{c2}^{c} \sim 1.05 - 1.1$) are consistent with the previous results obtained from magnetization and magnetoresistance measurements [11, 30–32], being on the lower end of the reported values for the H_{c2} anisotropy. The observation that H_{c2} is lower for the sample with lower RRR is broadly consistent with the results e.g. on $Y(Ni_{1-x}Co_x)_2B_2C$ [33] and $(Y_{1-x}Lu_x)Ni_2B_2C$ [34], however it disagrees with the generally expected increase of H_{c2} with decrease of the mean free path (decrease of RRR) expected for conventional superconductors (see [35] and references therein). Careful study, by several techniques, of H_{c2} and its anisotropy in RNi_2B_2C and in particular in YNi_2B_2C as a function of its mean free path is a topic of interest for a separate study.

A striking feature in high field magnetostriction of the sample A is clearly seen quantum oscillations (figure 6(a)), that start in the still superconducting, irreversible, region (at

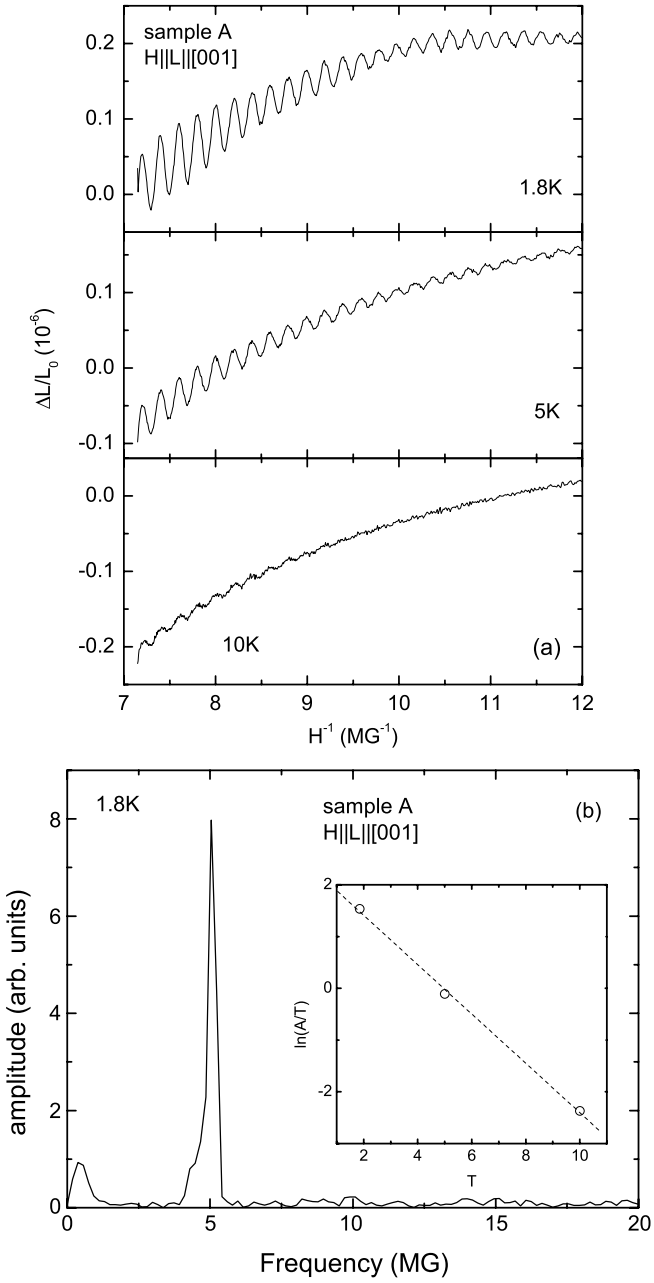

Figure 8. (a) Quantum oscillations of the longitudinal magnetostriction plotted as a function of $1/H$ for sample A. (b) Fourier transform of the $\Delta L/L_0$ versus $1/H$ curve for $T = 1.8$ K. Inset: $\ln(A/T)$ versus T plot for amplitude A at $H \sim 133$ kOe.

approximately 0.7 H_{c2} at $T = 1.8$ K) and continue, with growing amplitude, in higher fields (similarly, the oscillations are present for the sample B, but the Y scale in figure 6(b) does not allow to see them, see below). Quantum oscillations in magnetostriction is a known, albeit not so common phenomenon [36, 37], that requires high quality crystals and sensitive

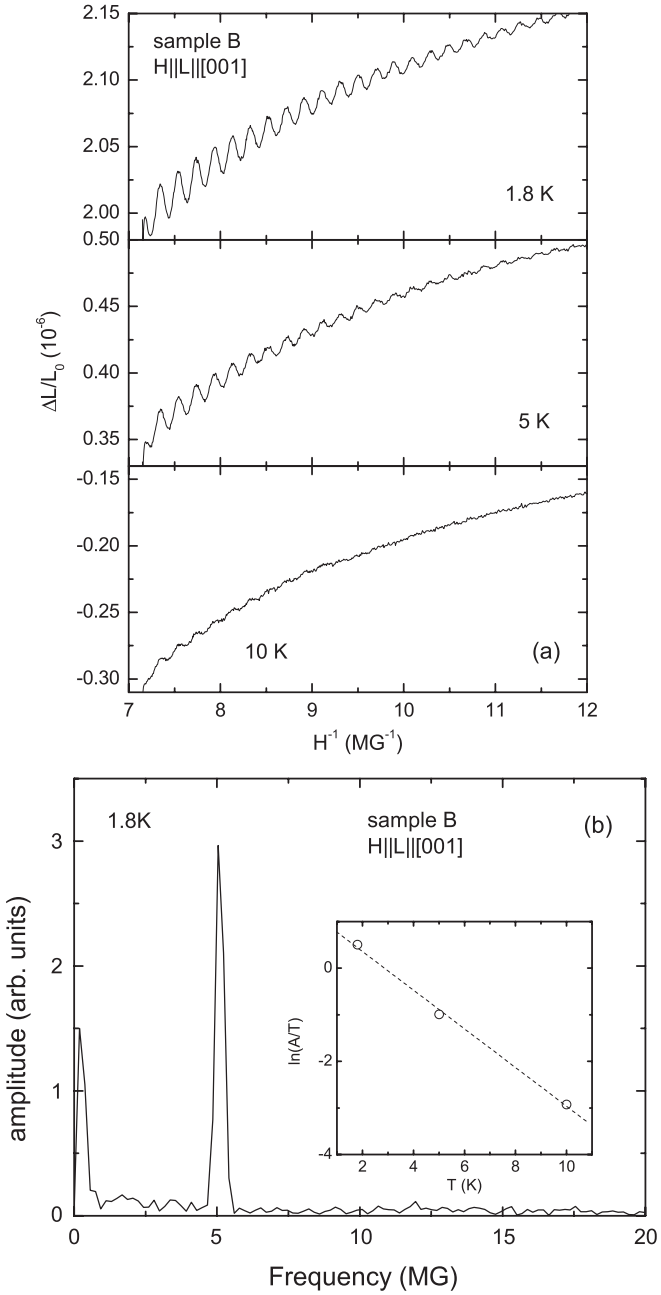

Figure 9. (a) Quantum oscillations of the longitudinal magnetostriction plotted as a function of $1/H$ for sample B. (b) Fourier transform of the $\Delta L/L_0$ versus $1/H$ curve for $T = 1.8$ K. Inset: $\ln(A/T)$ versus T plot for amplitude A at $H \sim 133$ kOe.

measurement techniques to be observed. These oscillations are present, with smaller amplitude, at least up to $T = 10$ K and are observed as well in the sample B. Magnetostriction data as a function of inverse magnetic field for three different temperatures are shown in figures 8(a)

(sample A) and 9(a) (sample B). At base temperature the amplitude of the oscillations for the sample A is ∼4 times higher, consistent with lower scattering in this sample. The Fourier transformation of the data (figures 8(b), 9(b)) reveals one frequency, $F = 5.04$ MG. The effective mass, m^*, corresponding to this orbit can be estimated from the slope of the $\ln(A/T)$ versus T plot (A—amplitude of the oscillations in some chosen field) [37]. For samples A and B this procedure results in values 0.38 m_0 and 0.43 m_0 respectively; in average: $m^* = 0.4 \pm 0.03 m_0$. Quantum oscillations in magnetization (de Haas–van Alphen effect) in YNi_2B_2C were described in number of publications (see e.g. [38–40] and references therein). The aforementioned oscillations in magnetostriction are consistent, both in frequency and effective mass values, with the strongest frequency observed by a conventional de Haas–van Alphen effect measurements, the α orbit on the Fermi surface part formed by the 17th band.

4. Summary

In summary, the TE measurements allow us to estimate uniaxial pressure derivatives of T_c which have different signs for pressure applied in the ab plane and along the c axis. The results call for re-evaluation of the role of NiB_4 structural unit on superconductivity in YNi_2B_2C. The irreversible MS in YNi_2B_2C is large, complex, has features associated with the peak (and/or 'dip') effect near T_c and is open for further, detailed studies of pinning. Quantum oscillations in MS (analogue of de Haas–van Alphen effect) were observed for $H \parallel c$. The frequency was identified as the α orbit previously seen in magnetization. If combined with high field magnetization measurements on the same crystals, the oscillatory MS will allow for estimate of evolution of the extremal orbit area under uniaxial stress [36].

Acknowledgments

We thank A Kreyssig for help in Laue-orienting floating zone grown crystal and M E Tillman for writing software interfacing a capacitance bridge with a PPMS environment. We appreciate the assistance of B N Harmon in the evaluation of Horton Norton and confirmation of our initial results. Ames Laboratory is operated for the US Department of Energy by Iowa State University under Contract No. W-7405-Eng.-82. This work was supported by the director for Energy Research, Office of Basic Energy Sciences. One of us (GMS) is supported by the National Science Foundation under DMR-0305397.

References

[1] Canfield P C, Gammel P L and Bishop D J 1998 *Phys. Today* **51** (10) 47
[2] Müller K-H and Narozhnyi V N 2001 *Rep. Prog. Phys.* **64** 943
[3] Müller K-H, Fuchs G, Drechsler S-L and Narozhnyi V N 2002 *Handbook of Magnetic Materials* vol 14, ed K H J Buschow (Amsterdam: North-Holland) p 199
[4] Bud'ko S L and Canfield P C 2006 *C. R. Phys.* **7** 56
[5] Fülber K, Geerkens A, Ewert S and Winzer K 1998 *Physica* C **299** 1
[6] Belger A, Jaenicke-Rössler U, Lipp D, Wehner B, Paufler P and Behr G 1998 *Physica* C **306** 277
[7] Jaenicke-Rössler U, Paufler P, Zahn G, Geupel S, Behr G and Bitterlich H 2002 *J. Alloys Compounds* **333** 28
[8] Meingast C, Blank B, Bürkle H, Obst B, Wolf T, Wühl H, Selvamanickam V and Salama K 1990 *Phys. Rev.* B **41** 11299
[9] Gugenberger F, Meingast C, Roth G, Grube K, Breit V, Weber T, Wühl H, Uchida S and Nakamura Y 1994 *Phys. Rev.* B **7** 56
[10] Sánchez D R, Bud'ko S L and Baggio-Saitovitch E M 2000 *J. Phys.: Condens. Matter* **12** 9941
[11] Xu M, Canfield P C, Ostenson J E, Finnemore D K, Cho B K, Wang Z R and Johnston D C 1994 *Physica* C **227** 321

[12] Canfield P C and Fisher I R 1994 *J. Cryst. Growth* **225** 155
[13] Miao X Y, Bud'ko S L and Canfield P C 2002 *J. Alloys Compounds* **338** 13
[14] Schmiedeshoff G M 2006 in preparation
[15] Kroeger F R and Swenson C A 1977 *J. Appl. Phys.* **48** 853
[16] Lawrie D D and Frank J P 1994 *Physica* C **245** 159
[17] Cheon K O, Fisher I R and Canfield P C 1999 *Physica* C **312** 35
[18] Schmidt H and Braun H F 1994 *Physica* C **229** 315
[19] Murayama C, Mori N, Takagi H, Eisaki H, Mizuhashi K, Uchida S and Cava R J 1994 *Physica* C **235–240** 2545
[20] Alleno E, Neumeier J J, Thompson J D, Canfield P C and Cho B K 1995 *Physica* C **242** 169
[21] Looney L, Gangopadhyay A K, Klehe A-K and Schilling J S 1995 *Physica* C **252** 199
[22] Kobayashi Y, Iwata M, Okamoto T, Takeya H, Kuroki K, Suzuki M and Asai K 2006 *Physica* B **378–380** 475
[23] Mattheiss L F, Siegrist T and Cava R J 1994 *Solid State Commun.* **91** 587
[24] Ikuta H, Kishio K and Kitazawa K 1994 *J. Appl. Phys.* **76** 4776
[25] Eremenko V V, Sirenko V A, Szymczak H and Nabialek A 1999 *Low Temp. Phys.* **25** 225
[26] Johansen T H 2000 *Supercond. Sci. Technol.* **13** R121
[27] Gerber A 2001 *Modern Trends in Magnetostriction Study and Application* ed M R J Gibbs (Dordrecht: Kluwer) p 151
[28] Johansen T H, Lothe J and Bratsberg H 1998 *Phys. Rev. Lett.* **80** 4758
[29] Kogan V G 2006 in preparation
[30] Du Mar A C, Rathnayaka K D D, Naugle D G and Canfield P C 1998 *Int. J. Mod. Phys.* B **12** 3264
[31] Bud'ko S L, Kogan V G and Canfield P C 2001 *Phys. Rev.* B **64** 180506R
[32] Wimbush S C, Schultz L and Holzapfel B 2004 *Physica* C **408–410** 83
[33] Cheon K O, Fisher I R, Kogan V G, Canfield P C, Miranovic P and Gammel P L 1998 *Phys. Rev.* B **58** 6463
[34] Rathnayaka K D D, Naugle D G, Dumar A C, Anatska M P and Canfield P C 2003 *Int. J. Mod. Phys.* B **17** 3493
[35] Helfand E and Werthamer N R 1966 *Phys. Rev.* **147** 288
[36] Chandrasekhar B S and Fawcett E 1971 *Adv. Phys.* **20** 775
[37] Shoenberg D 1984 *Magnetic Oscillations in Metals* (Cambridge: Cambridge University Press)
[38] Winzer K and Krug K 2001 *Rare Earth Transition Metal Borocarbides (Nitrides): Superconducting, Magnetic and Normal State Properties* ed K-H Müller and V Narozhnyi (Dordrecht: Kluwer) p 63
[39] Yamauchi K, Katayama-Yoshida H, Yanase A and Harima H 2004 *Physica* C **412–414** 225
[40] Ignatchik O, Coffey T, Hagel J, Jaeckel M, Jobiliong E, Souptel D, Behr G and Woznitsa J 2005 *J. Magn. Magn. Mater.* **290/291** 424